View Online / Journal Homepage
Dynamic Article Links

Journal of Materials Chemistry

Cite this: DOI: 10.1039/c2jm33784c

www.rsc.org/materials

FEATURE ARTICLE

Graphene-based transparent flexible electrodes for polymer solar cells

Ming He,[a] Jaehan Jung,[b] Feng Qiu[a] and Zhiqun Lin*[b]

Received 13th June 2012, Accepted 12th July 2012
DOI: 10.1039/c2jm33784c

Conjugated polymer-based bulk heterojunction (BHJ) solar cells are widely recognized as a promising alternative to their inorganic counterparts for achieving low-cost, roll-to-roll production of large-area flexible lightweight photovoltaic devices. Current research in designing new polymers and optimizing device architectures has been devoted to improving the film morphology, photovoltaic performance and stability of polymer BHJ solar cells. Conjugated block copolymers (BCPs), including rod–coil and rod–rod BCPs, exhibit excellent flexibility for tuning the bandgap of semiconductor polymers, regulating the molecular organization of donor (and/or acceptor) units, templating the film morphology of active layers, and achieving well-defined BHJ architectures. In this Feature Article, we summarize the recent developments over the past five years in the synthesis, self-assembly, and utilization of conjugated rod–coil and all-conjugated rod–rod BCPs for solar energy conversion; highlight the correlation between the microphase-separated morphology and photovoltaic properties in conjugated BCPs; and finally provide an outlook on the future of BCP-based photovoltaic devices.

1. Introduction

Polymer solar cells have been widely recognized as a promising low-cost alternative to conventional inorganic solar cells that often require expensive processing. They capitalize on many advantageous attributes peculiar to conjugated polymers (CPs), such as light weight, flexibility, non-vacuum processability (*e.g.*, spin-coating and inkjet printing), roll-to-roll production, low cost, and large area.[1–9] The most effective architecture of polymer solar cells is the bulk heterojunction (BHJ) where efficient charge separation is enabled by a large-area donor–acceptor interface.[10] Such heterojunction photovoltaics are engineered to overcome the intrinsic limitations to photocurrent generation in CPs, which are short exciton diffusion lengths, relatively large exciton binding energies, and low electron mobilities.[11] The power conversion efficiency (PCE) of polymer BHJ solar cells largely depends on the energy-level alignment of the donor and acceptor materials and the nanostructured photoactive layer,[12–14] that is,

[a]*State Key Laboratory of Molecular Engineering of Polymers, Ministry of Education, Department of Macromolecular Science, Fudan University, Shanghai 200433, China*
[b]*School of Materials Science and Engineering, Georgia Institute of Technology, Atlanta, GA, 30332, USA. E-mail: zhiqun.lin@mse.gatech.edu*

Ming He

Ming He received the Ph.D. degree in Polymer Chemistry and Physics from Fudan University of China in 2011 under the supervision of Professor Feng Qiu. He worked with Professor Zhiqun Lin at Iowa State University of USA as a visiting student from 2009 to 2011. He is currently a postdoctoral researcher at Fudan University. His research interests include conjugated polymers, block copolymers, quantum dots, polymer solar cells, dye-sensitized solar cells, graphene electrode materials, and thermoelectrical nanocomposites.

Jaehan Jung

Jaehan Jung received the B.S. degree in Materials Science and Engineering from Seoul National University, Republic of Korea in 2010. He is currently a PhD candidate in Materials Science and Engineering at Georgia Institute of Technology studying under Prof. Zhiqun Lin. His current research interests include graphene, inorganic nanoparticles, and their application in photovoltaic devices.

(a) a large energy offset between the highest occupied molecular orbital (HOMO) of the donor material and the lowest unoccupied molecular orbital (LUMO) of the acceptor material to maximize the open-circuit voltage (V_{oc}), (b) a low bandgap CP donor material to increase the short-circuit current density (J_{sc}), and (c) a fine scale of phase separation between the donor and acceptor domains with bicontinuous charge pathways inside the active layer to enhance J_{sc} and the fill factor (FF).[15–18] Recent advances in rationally designing new low bandgap CPs and engineering BHJ nanostructures render the improved performance of polymer BHJ solar cells, which has exceeded 8%.[19–21] However, the use of indium tin oxide (ITO) as a transparent electrode limits the realization of low-cost, flexible, and stable polymer solar cells.[22]

ITO is a heavily doped n-type semiconductor with a large bandgap (*i.e.*, 3.5–4.3 eV). It is highly transparent in the visible region of the light spectrum.[23] The ITO deposited on glass substrates by electron beam evaporation, chemical vapor deposition, or magnetron sputter deposition is commonly used as the transparent electrode in polymer solar cells due to its high transparency (>90%) at the wavelength of 550 nm, low electrical resistance (<100 Ω per square), and favorable work function (*i.e.*, 4.5–5.2 eV).[24–27] However, the low abundance of indium and high cost of ITO ($1000 per kilogram) prevent ITO electrodes from being used in large-scale manufacturing.[22] Additionally, other constraints of ITO electrodes include (a) a complicated electrode deposition process, (b) brittle rupture characteristic, making it not suitable for being used in flexible polymer solar cells, (c) chemical instability in the acid environment, and (d) poor transparency in the near-IR region of the light spectrum.[28] In this context, the development of alternatives to replace conventional ITO electrodes is of great importance in achieving low-cost, large-area, and flexible polymer solar cells. Recent research has witnessed rapid progress in seeking new transparent flexible electrodes, such as silver nanowires,[29–31] conductive polymers,[32,33] and carbon nanotubes (CNTs),[34,35] which benefit primarily from the combination of their high transparency in a broad range of the light spectrum and their low resistance comparable to that of ITO.

Despite the exciting progresses noted above, the research is still in its early stage. Several intrinsic and extrinsic variables need to be delicately tailored to improve the device performance.[36,37] In an ideal polymer BHJ solar cell composed of a transparent ITO glass, an anode buffer layer, a photoactive layer, a cathode buffer layer, and a top metal electrode (Fig. 1a), the thoroughly mixed donor material (*i.e.*, CPs) and acceptor material (*i.e.*, fullerene derivatives) are expected to generate a large donor–acceptor interfacial area for effective exciton dissociation, where the dimensions of both the donor and acceptor phases are within the exciton diffusion length (~10 nm) to allow excitons to effectively diffuse to the donor–acceptor interface driven by the energy-level difference between the two semiconductors. The nanophase separation of donors and acceptors should form an interpenetrating network to promote fast transport of free electrons and holes to their respective electrodes driven by the work function difference between a transparent electrode and a metal electrode.[7,15] The PCE of polymer solar cells is dictated by the efficiency of fundamental photophysical processes, including light absorption, exciton diffusion, exciton dissociation, charge transport and charge collection (Fig. 1b).[38] The intrinsic property of electrode materials and the extrinsic property of the photoactive layer–electrode interface play a crucial role in these photophysical processes. The efficiency of light absorption is related to the transparency of the electrode material, the efficiency of charge transport is correlated to the leakage path to the electrodes, and the efficiency of charge collection is associated with the sheet resistance of the electrode.[36] Moreover, the nature of chemical compatibility and physical contact between the photoactive layer and the transparent electrode may also influence the nanostructures of the photoactive layer, the optoelectronic process, and thus the PCE.[36]

Feng Qiu

Feng Qiu received the Masters degree in Engineering from Shanghai Institute of Metallurgy, Chinese Academy of Sciences in 1995, and the PhD degree in Polymer Chemistry and Physics from Fudan University in 1998. He was a postdoctoral research associate at University of Pittsburgh. In 2001 he joined Fudan University as an Associate Professor at the Department of Macromolecular Science, and was promoted to Professor in 2003. His research activities primarily involve the equilibrium and dynamical properties of complex block copolymers, polymer solutions, thin films, and graphene. He received China National Funds for Distinguished Young Scientists in 2006.

Zhiqun Lin

Zhiqun Lin received the Masters degree in Macromolecular Science from Fudan University, Shanghai in 1998, and the PhD degree in Polymer Science and Engineering from UMass, Amherst in 2002. He was a postdoctoral associate at UIUC. He joined the Department of Materials Science and Engineering at Iowa State University in 2004, and was promoted to Associate Professor in 2010. He moved to Georgia Institute of Technology in 2011. His research interests include polymer solar cells, dye-sensitized solar cells, graphene, quantum dots (rods), conjugated polymers, block copolymers, polymer blends, hierarchical structure formation and assembly, surface and interfacial properties, and multifunctional nanocrystals. He is a recipient of an NSF Career Award.

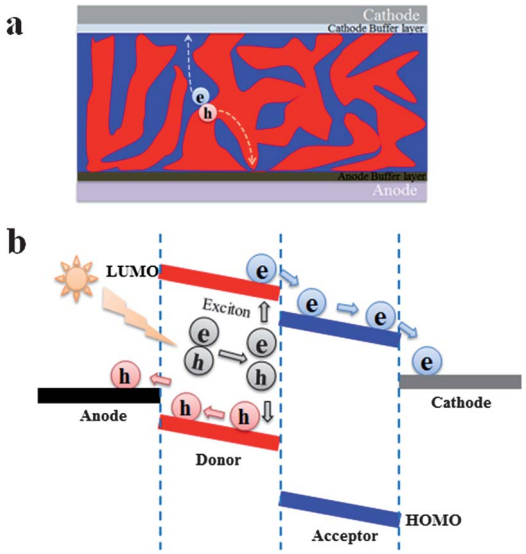

Fig. 1 (a) The device architecture of polymer bulk heterojunction (BHJ) solar cells, the red and blue domains correspond to the donor and acceptor phases, respectively. (b) Simplified schematic showing the principal internal processes that take place in polymer BHJ solar cells. Adapted with permission from ref. 38, Copyright© 2010 Elsevier Ltd.

The discovery of graphene consisting of a single layer of carbon atoms arranged in two-dimensional (2D) honeycomb lattices provided new opportunities for the development of alternative transparent electrodes. Graphene is the basic building block for some carbon allotropes and can be wrapped up into zero-dimensional (0D) fullerene, rolled into one-dimensional (1D) CNT, or stacked into multilayer three-dimensional (3D) graphite.[39] Distinctly different from its carbon allotropes, graphene possesses superior physical properties, including a specific surface area of $\sim 2.6 \times 10^3$ m^2 g^{-1},[40] carrier mobility of 2×10^5 cm^2 V^{-1} s^{-1},[41] Young's modulus of 1×10^3 GPa,[42] and fracture strength of 125 GPa.[43] These outstanding properties have led to various practical applications of graphene materials as supercapacitors,[40] Li-ion batteries,[44] dopants,[45] noble-metal free electrocatalysts,[46] dispersible carriers for catalysis,[47] templates for chemical reactions,[48] and so on. Of particular interest is the combination of good optical transmittance, electrical conductivity, chemical stability, and flexibility allowing the development of graphene electrodes.[49] Efforts towards better controlled synthesis, surface functionalization, and device fabrication are expected to further improve the performance of graphene electrodes, which include (a) tuning the energy-level alignment of the photoactive layer–graphene interface for an effective Ohmic contact, (b) modifying the hydrophilic character of graphene for a uniform coating of the photoactive layer, (c) engineering the surface optical effect for an enhanced light harvesting, and (d) improving the electrode stability for a long-term use.[36] In this Feature Article, we summarize recent advances in the preparation, modification, and application of graphene-based transparent electrodes in polymer solar cells; highlight the effects of graphene morphology, transparency, sheet resistance, and chemical compatibility on photovoltaic performance; and finally provide an outlook on the future development of graphene electrodes.

2. Preparation of graphene electrodes

2.1 CVD growth of graphene

Direct growth of large-area, high-quantity, continuous graphene by chemical vapor deposition (CVD) with very few structural defects promises the use of graphene as electrodes in polymer solar cells.[50] Recently, a monolayer of 30 inch graphene film has been produced by the CVD method on Cu catalyst substrates that are held at 1000 °C, followed by wet-chemical doping. The resulting film has a low sheet resistance of ~125 Ω per square as well as a high optical transmittance of 97.4%. Multilayer graphene (*i.e.*, 2–5 layers) can be prepared by the layer-by-layer (LBL) CVD method. For example, a four-layer graphene exhibits an even lower sheet resistance of ~30 Ω per square with an optical transmittance of ~90%. These high-quality graphene films have been successfully fabricated into fully functional touch-screen panel devices.[51] Ni, Pt and Ru can also be used as catalyst substrates for the CVD growth of graphene.[52–55] The growth processes of graphene on Cu and Ni are different which can be ascribed to the solubility difference of carbon atoms in these two metals: a large amount of carbon atoms diffuse, mix, segregate and/or precipitate at the Ni surface because of its high carbon solubility, while graphene on the Cu surface grows by absorbing a small amount of carbon atoms on the surface due to its low carbon solubility.[56] Actually, the low carbon solubility of Cu is beneficial to controlling the uniform growth of graphene on the substrate,[57] thereby avoiding the precipitation of extra carbons to form thick graphite during the cooling-down process of CVD.

Etching the metal substrate and transferring the CVD-grown graphene to target substrates for electronic device fabrication is another important procedure. $FeCl_3$ is the most widely used etchant for Cu and Ni substrates, because it effectively etches the metal *via* a moderate redox reaction without forming gaseous outcomes or precipitates. The ion residues are then removed by rinsing with diluted HCl and deionized water to prevent unintentional doping of graphene.[58] In contrast, the chemical reaction of etching Cu with nitric acid will form hydrogen bubbles in the solution, which may cause cracks in graphene.[50] Polymer substrates (*i.e.*, poly(methyl methacrylate) (PMMA) or polydimethylsiloxane (PDMS)) are then used as protective stamps to attach graphene grown on the metal substrates.[59–61] After etching the metal substrates, only the graphene film is left on the soft polymer substrate, which is subsequently transferred to the target substrate of electronic devices, followed by removing the polymer substrate in organic solvents (*e.g.*, acetone, tetrahydrofuran, chloroform, *etc.*).[61,62] Fig. 2 illustrates a typical procedure for the synthesis, etching and transferring of a CVD-grown graphene film, where the patterned-graphene film is prepared on a pre-patterned Ni substrate and two different transfer methods are used.[62] It is noteworthy that the solvent-etching process to remove polymer substrates (*i.e.*, PMMA or PDMS) may tear the graphene film, and the resulting graphene film may also suffer from insulating polymer residues. Two alternative etching approaches are thus suggested: (a) briefly dipping the polymer substrate in acetone for 2 min followed by acetone vapor annealing for 3 h and (b) thermally annealing the polymer substrate for 3 h at 500 °C under mixed gas of hydrogen–argon.[58]

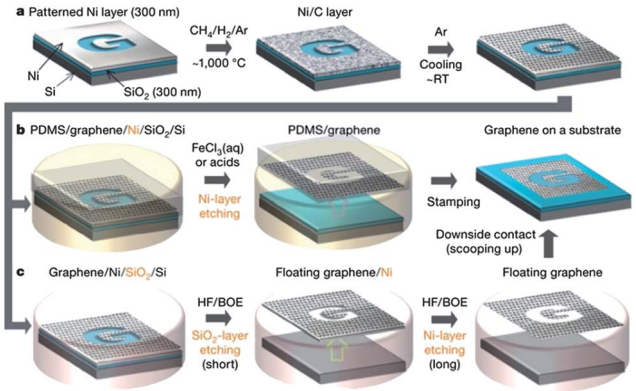

Fig. 2 Synthesis, etching, and transferring processes of the large-scale and patterned graphene films. (a) Synthesis of patterned graphene films on thin nickel layers. (b) Etching by the use of $FeCl_3$ (or acids) and transferring of graphene films by using a polydimethylsiloxane (PDMS) stamp. (c) Etching by the use of buffered oxide etchant (BOE) or hydrogen fluoride (HF) solution and transferring of graphene films. Adapted with permission from ref. 62, Copyright© 2009 Nature Publishing Group.

The performance of transparent electrodes is quantified by the figure of merit, $\sigma/\alpha = -[R_s\ln(T + R)]^{-1}$, in which σ is the electrical conductivity, α is the absorption coefficient, R_s is the sheet resistance, T is the transmittance, and R is the reflectance.[63] A higher σ/α corresponds to a better performance of the electrode. The σ/α of ITO glass is $\sim 4\ \Omega^{-1}$. For the graphene electrode, it is still difficult to accurately calculate and compare its σ/α value in previous work because of the rare measurements of absorption and reflectance coefficients. Thus, an approximate figure of merit, $\sigma_{op}/\sigma_{dc} = Z_0/2R_s(T^{-0.5} - 1)$, is suggested to evaluate the performance of graphene electrodes based on the reported data, where $\sigma_{dc} = R_sL$ is the electrical conductivity, L is the film thickness, and σ_{op} is the optical conductivity correlated to the T through $T = (1 + Z_0\sigma_{op}L/2)^{-2}$, where Z_0 is the impedance of free space (*i.e.*, 377 Ω for graphene).[64] Similar to the σ/α, a higher value of σ_{op}/σ_{dc} corresponds to a better performance of the electrode. Fig. 3a summarizes the transmittance and sheet resistance data in the literature, in which graphene films are prepared either by CVD, reduced graphene oxide, chemically modified graphene, pristine exfoliated graphene, or chemical synthesis.[64] The values of σ_{dc}/σ_{op} calculated from the T and R_s data are shown in Fig. 3b. The minimum industry standard for the application of transparent electrodes requires a sheet resistance of <100 Ω per square with an optical transmittance of >90%, corresponding to the σ_{dc}/σ_{op} value of 35. The high-quality graphene film prepared by CVD exhibits the highest σ_{dc}/σ_{op} value of ~10 as compared to those prepared by other methods. It is worth noting that a potential σ_{dc}/σ_{op} value of 330 is predicted for the doped graphene, which is high enough for graphene to be used as a transparent electrode in any organic electronics.

As discussed above, the CVD-grown graphene films can achieve a high performance (*i.e.*, $\sigma_{dc}/\sigma_{op} = \sim 10$) with the sheet resistance ranging from 230 Ω per square with an optical transmittance of ~72% to 8300 Ω per square with an optical transmittance of ~90%, which is almost comparable to that of mechanically cleaved graphene.[53,65,66] The high performance of CVD-grown graphene can be attributed to the low-density

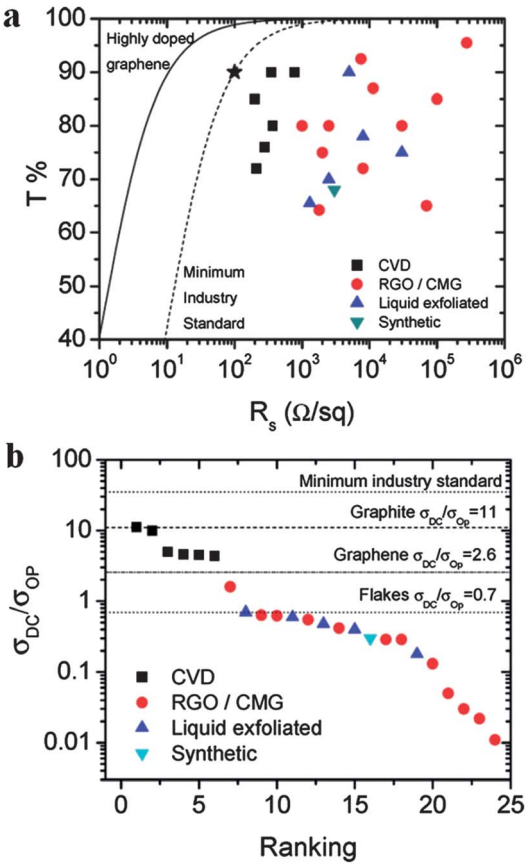

Fig. 3 (a) Transmittance and sheet resistance of graphene films reported in the literature. The graphene films were prepared either by chemical vapor deposition (CVD), reduced graphene oxide (rGO), chemically modified graphene (CMG), pristine exfoliated graphene, or chemical synthesis. The star represents the minimum industry standard for transparent electrodes ($R_s = 100\ \Omega$ per square, $T = 90\%$), corresponding to $\sigma_{dc}/\sigma_{op} = 35$. The dashed line illustrates the set of (T, R_s) data consistent with $\sigma_{dc}/\sigma_{op} = 35$. The solid line corresponds to the calculated case of highly doped graphene ($\sigma_{dc}/\sigma_{op} = 330$). (b) The conductivity ratio, σ_{dc}/σ_{op}, is calculated from T and R_s data as mentioned above. The same symbols in each figure present varied values of graphene electrodes prepared by the same method reported in different literature. Adapted with permission from ref. 64, Copyright© 2010 American Chemical Society.

defects and low contact resistance of grain boundaries during *in situ* CVD. The OPV device with the structure of CVD-grown graphene/PEDOT:PSS/CuPc/C_{60}/Al exhibits comparable performance to those of ITO-based devices.[65] Graphene can also be utilized as the top electrode in the inverted P3HT:PCBM-based devices, resulting in the PCE of ~2.5%.[67] Intriguingly, CVD-grown graphene electrodes perform much better than ITO electrodes in terms of mechanical flexibility. Fig. 4 compares the photovoltaic performances of CVD-grown graphene and ITO electrodes under the bending conditions. The graphene-based devices possess an outstanding ability to work under bending up to 138°; this contrasts the ITO-based devices that break up below 60°. The cracks formed on the ITO electrode after bending are shown in Fig. 4d, while the graphene electrode remains intact.[65] The sheet resistance of CVD-grown graphene can be mostly restored after stretching, further suggesting its excellent mechanical stability.[53]

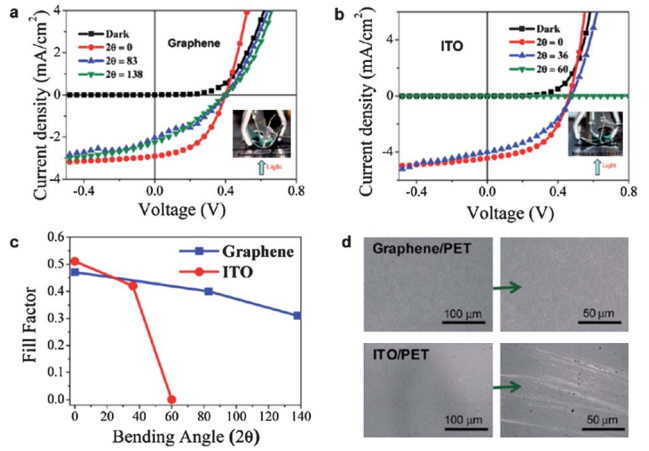

Fig. 4 Current density–voltage (*J–V*) characteristics of (a) graphene-based photovoltaic cells and (b) ITO-based photovoltaic cells under 100 mW cm^{-2} AM 1.5G spectral illumination at different bending angles. Insets show the experimental setup employed in the experiments. (c) Fill factor dependence on the bending angle for the graphene and ITO devices. (d) SEM images showing the surface structure of graphene (top) and ITO (bottom) photovoltaic cells after being subjected to the bending angles described in (a) and (b). Adapted with permission from ref. 65, Copyright© 2010 American Chemical Society.

2.2 Exfoliation of graphene oxide

In order to achieve the widespread use of graphene electrodes, rather than the expensive CVD method, an effective route to prepare large quantities of graphene is required. The 2010 Nobel Prize in Physics was awarded to Andre Geim and Konstantin Novoselov for their groundbreaking experiments on the two-dimensional graphene material, which was obtained from simple mechanical exfoliation of graphite using the 'Scotch tape' method.[66,68] Graphite is a stack of multilayer graphene, which is likely the most available and least expensive source for a large-scale production of graphene. As most of the unique properties are only associated with single- or few-layer graphene, it is crucial to prevent the aggregation of graphene by resisting to the strong van der Waals interactions.[69–71] To this end, a novel chemical exfoliation of graphite oxide (GO) has emerged as a standard solution-based method to prepare large quantities of graphene from graphite,[70,72] which involves (a) the chemical oxidation of graphite to GO in the mixture of concentrated H_2SO_4 and $KMnO_4$ by a modified Hummer's method,[73,74] (b) the exfoliation of hydrophilic GO through ultrasonication or mechanical stirring for a long period of time,[70,75] and (c) the conversion of as-exfoliated GO sheets to conductive graphene by chemical reduction,[76–79] thermal annealing treatment,[80–82] or an ultraviolet-assisted method.[71] GO is highly negatively charged with hydrophilic groups (*i.e.*, carboxyl acid, phenolic hydroxyl, epoxide, *etc.*).[83,84] As such, the interlayer distance of GO increases to 7.8 Å in comparison to that of 3.4 Å in the pristine graphite, and GO is readily exfoliated into single-layer sheets.[43,70] By delicately optimizing the pH of GO aqueous solution, a balanced electrostatic repulsion results in the stable aqueous dispersion of graphene colloids that are reduced from GO in the real time within the aqueous solution.[71] In addition, the sonication-driven exfoliation of graphite to graphene can be realized in organic solvents (*i.e.*, dimethylformamide (DMF), *N*,*N*-dimethylacetamide (DMA), and *N*-methylpyrrolidone (NMP)) without chemical oxidation. The exfoliation of graphite in organic solvents depends primarily on the strong interaction between the solvent and the interlayers of graphite. The main drawback of organic-phase exfoliation is the high boiling point of the organic solvent, making the electrode fabrication process more complicated.[49]

Owing to the ionization of carboxylic-acid and phenolic-hydroxyl groups, negatively charged GO forms stable colloids in water, thereby enabling the fabrication of GO films by facile solution-based processes, such as vacuum filtration, spray coating, dip coating, spin coating, and Langmuir–Blodgett (LB) assembly.[27,85,86] Spin coating is perhaps the simplest method to deposit nanoscale graphene films with controlled thicknesses from solution. In a typical process, GO in water, methanol, ethanol, or the mixed solvents is spin-coated on the substrate, which is pretreated by oxygen plasma to facilitate the hydrophilic contact between GO and the substrate. The thickness of the GO film is controlled by the solution concentration and the spin speed. The spin-coated GO films can be reduced to conductive graphene by chemical or thermal reduction. Fig. 5a and b show the performance of flexible P3HT/PCBM solar cells using chemically reduced GO (rGO) as bottom electrodes, which were spin-coated on the polyethylene terephthalate (PET) substrate.[87] The performance of these flexible devices is strongly correlated to the charge transport efficiency and the optical transmittance of rGO electrodes as a function of film thickness. The optimal thickness of rGO electrodes was about 16 nm, leading to the highest PCE of 0.78%. Similar to CVD-grown graphene electrodes, rGO electrodes prepared by chemical exfoliation also possessed good mechanical flexibility. The

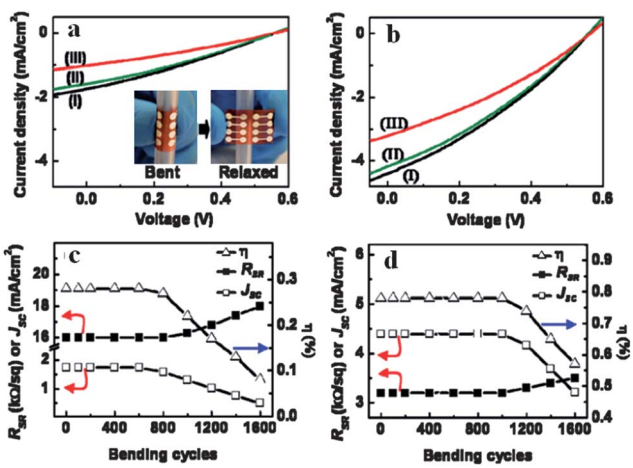

Fig. 5 Current density–voltage (*J–V*) characteristics of polymer photovoltaic devices on reduced GO electrodes under 100 mW cm^{-2} AM 1.5G simulated globe sun illumination: (a) the 4 nm rGO film after applying (I) 400, (II) 800, and (III) 1200 cycles of bending; (b) the 16 nm rGO film after applying (I) 800, (II) 1200, and (III) 1600 cycles of bending. The short-circuit current density (J_{sc}), power conversion efficiency (η), and the sheet resistance (R_{SR}) of device (a) and device (b) are plotted as a function of bending cycles in (c) and (d), respectively. Inset in (a): photograph of the bending–relaxing experiments of the polymer photovoltaic device. Adapted with permission from ref. 87, Copyright© 2010 American Chemical Society.

as-prepared flexible devices performed stably after the repeated bending and relaxing (Fig. 5c and d).

GO also serves well as an alternative to the PEDOT:PSS buffer layer. Because of the poor conductive properties of GO, the performance of P3HT/PCBM solar cells using GO as the anode buffer layer is related to the thickness of GO. The oxide groups destroy the carbon sp^2 structures and are responsible for the poor electrical conductivity of GO. Although hydrazine reduction is widely used to eliminate the oxide groups and recover the electronic properties of GO, the use of hydrazine is highly toxic.[88] The resulting PCE of ~3.5% of the hydrazine-reduced GO device is comparable to that of the device utilizing PEDOT:PSS as the buffer layer, however, it is challenging to fabricate a uniform buffer layer without leakage in a very thin rGO film (<2 nm).[89] Recently, a new reducing agent, *p*-toluenesulfonyl hydrazide, has been successfully applied to produce the reduced GO with improved conductive property and an optimized thickness of the rGO buffer layer around 5 nm. The resulting device showed an average V_{oc} of 0.59 V, J_{sc} of 9.33 mA cm^{-2}, FF of 66.7%, and PCE of 3.63%, which were highly comparable to those of the PEDOT:PSS-based device.[90] More importantly, the device displayed a much longer term use as compared to the PEDOT:PSS-based device, suggesting that rGO exhibited a more efficient passivation property against oxygen and moisture than PEDOT:PSS.[91]

The LB method that renders the self-assembly of amphiphilic molecules at the air–water interface under well-controlled compressing conditions provides another effective way to fabricate GO electrodes on a variety of substrates.[92–95] The electrostatic repulsion, arising from the ionization of carboxyl-acid and phenol-hydroxyl groups located at the edge of GO sheets, enables GO to form a stable colloidal dispersion in water against flocculation or coagulation.[86] The 2D water surface is a perfect platform for the fabrication of monolayer GO films without the need for surfactants or stabilizing agents. Additionally, the 2D water surface is geometrically similar to the GO film, making it ideal to accommodate flat GO sheets.[96] In principle, the LB method allows for the deposition of GO films on any arbitrary substrate, and the size of the film is only limited by the size of the LB trough.[49] By controlling the compression pressure and rate, a large area of GO monolayers can be obtained with desired film packing densities: the GO monolayer collected at an over-packed region based on the pressure–area isotherm exhibited a sheet resistance of 4000 Ω per square with an optical transmittance of ~95% after being thermally reduced at 500 °C, which is comparable to that of GO films prepared by spin coating;[86,97] and the rGO monolayer after chemical reduction showed a sheet resistance of 459 Ω per square with an optical transmittance of ~90%, corresponding to a remarkably high σ_{dc}/σ_{op} value of 7.29.[98]

2.3 Colloidal graphene quantum dots

Different from the micrometer-sized graphene with an infinite exciton Bohr radius, the effect of quantum confinement in nanoscopic graphene quantum dots (QDs) is expected to induce remarkably new features for graphene. The magneto-optical spectrum of graphene QDs lies in the range of 0–3 eV, suggesting that graphene QDs are also very suitable for carbon-based electronic applications.[99] The size-dependent bandgap and large optical absorbance of graphene QDs are particularly advantageous for use as transparent electrodes.[100] Compared to the top-down cutting of graphene sheets to prepare graphene QDs,[101,102] the bottom-up oxidative condensation provides a facile route to synthesizing graphene QDs. The principle of the oxidative-condensation reaction of graphene QDs includes: (a) the oxidation of polyphenylene dendritic precursors through stepwise reactions, (b) the stabilization of graphene QDs through the covalent attachment of multiple 2′,4′,6′-trialkyl phenyl groups, and (c) the extension of the alkyl chains on the edge of graphene QDs to prevent them from aggregating (Fig. 6).[103,104] The as-synthesized graphene QDs are highly soluble in common organic solvents (*e.g.*, chloroform, toluene, THF, *etc.*). The Langmuir techniques are suggested to control the self-assembly of graphene QDs and further fabricate them into thin-film electrodes.[105] The graphene QDs may also be fabricated into electrode films by thermal fusion at high temperature, which has been used to construct graphene electrodes from the nano-graphene molecules of giant polycyclic aromatic hydrocarbons (PAHs). A PCE of 0.29% in P3HT:PCBM solar cells was achieved by capitalizing on the PAH–graphene film as anode electrodes.[35]

3. Engineering the functions of graphene electrodes

3.1 Chemical doping of graphene

Graphene is a zero-gap semiconductor because its conical conduction band and valence band meet at the Dirac point,

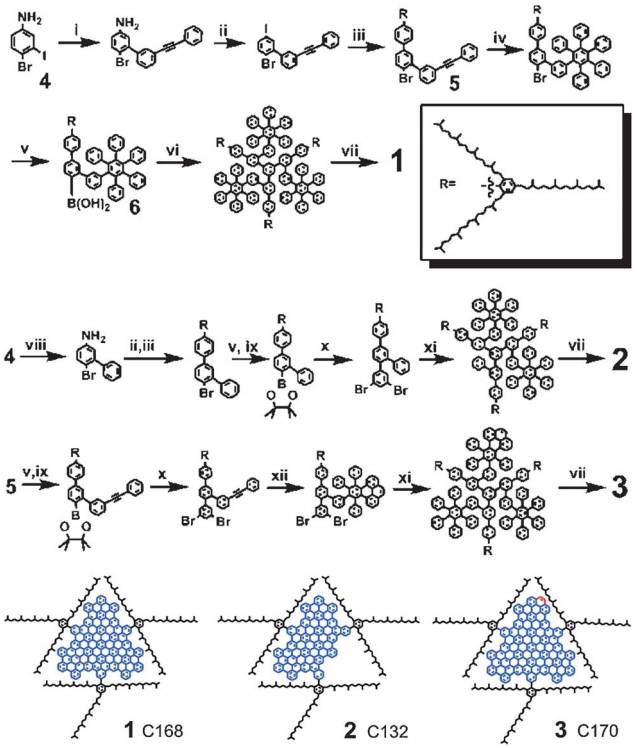

Fig. 6 Synthesis of colloidal graphene quantum dots *via* the oxidative condensation. Adapted with permission from ref. 103, Copyright© 2010 American Chemical Society.

where the carrier density is vanishes.[106–108] Owing to unintentional structural defects and impure dopants, the Fermi level of graphene prepared by chemical or physical exfoliation will not actually reside at the Dirac point, thereby generating a very low carrier density and thus a high sheet resistance.[109] To date, even if the quality of graphene is very high, the electrical conductivity of CVD-grown graphene (*e.g.*, 2100 Ω per square at 97% transmittance) is still not high enough for the application in transparent electrodes.[110] Two approaches have been explored to increase the electrical conductivity of graphene, namely, chemical doping and LBL stacking of multilayer graphene. As a high transmittance is highly desirable for transparent electrodes, chemical doping is a promising route to graphene electrodes with high conductivity and high transmittance. Nitric acid is a typical p-type dopant for graphene, in which an electron is transferred from graphene to nitric acid, forming a charge-transfer complex as follows:

$$6HNO_3 + 25C \rightarrow C_{25}^{+}NO_3^{-}\cdot 4HNO_3 + NO_2 + H_2O$$

Compared to the doping of multilayer graphene, the interlayer doping of graphene yields better optical and electrical properties. For example, a low sheet resistance of 90 Ω per square with an optical transmittance of ~80% was achieved in an 8-layer stacked graphene film.[109] $AuCl_3$ can also be used as the doping agent for graphene, which results in up to ~77% decrease in the sheet resistance with only 2% decrease in transmittance as compared to the pristine graphene.[111] Furthermore, graphene films doped by $AuCl_3$ become more hydrophilic and suitable for the spin-coating of PEDOT:PSS.[112] An $HAuCl_4$-doped graphene monolayer was used as the top electrode in an inverted P3HT:PCBM solar cell, where Au nanoparticles with an average diameter of 30 nm were generated on the graphene film, leading to a high PCE of 2.7% over a large area of illumination (*i.e.*, ~20 mm^2).[113]

Organic residues formed in the doping and transfer processes of CVD-grown graphene are detrimental to the conductivity, transparency, and morphology of graphene electrodes, an interlayer-coupling method is then developed to reduce contaminations from organic residues.[114] As shown in Fig. 7, a PMMA-coated graphene monolayer was directly transferred onto another graphene monolayer grown on the Cu substrate by CVD. The π–π interactions between these two graphene layers bonded them together when thermally annealed at 120 °C. After etching the Cu substrate, the bilayer graphene can be directly transferred onto a third graphene monolayer grown on the Cu substrate to form a three-layer graphene film. After repeated transferring, annealing, and etching steps, a multilayer graphene film can be transferred to the target substrate, followed by removal of the top PMMA with acetone. HCl was used to dope each graphene monolayer during the transfer process, followed by doping the top surface of the graphene film with HNO_3 after removing PMMA. The resulting four-layer graphene film showed a sheet resistance of ~80 Ω per square with an optical transmittance of ~90% at 550 nm, which was better than that made by wet transferring (*i.e.*, 90 Ω per square at 80% transmittance). In order to exploit this multilayer graphene as the electrode in P3HT:PCBM solar cells, a thin layer of MoO_3 (~2 nm) was evaporated on the graphene to improve its hydrophilicity for uniform coating of PEDOT:PSS. The performance of the graphene-based device was about 2.5%, comparable to that of the device using the ITO as the electrode.

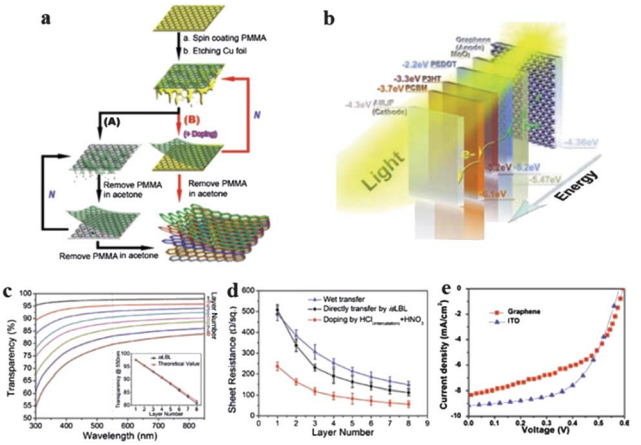

Fig. 7 (a) Schematic drawing of multilayer graphene films made by: (A) normal wet transfer and (B) interlayer-coupling assembly. (b) Schematic diagram of a photovoltaic device structure. (c) UV-vis spectra of layer-by-layer (LBL) stacked graphene films; the inset compares the transparency of the LBL stacked graphene film and its theoretical value at 550 nm. The transparency of the graphene film decreases with the increase of the graphene layer. (d) Comparison of sheet resistance as a function of layer number for graphene films prepared using wet transfer, LBL, and LBL acid-doped methods. (e) Current density–voltage (*J*–*V*) characteristics of anode/PEDOT:PSS/P3HT:PCBM/LiF/Al (the anode is ITO or MoO_3-coated graphene). Adapted with permission from ref. 114, Copyright© 2011 Wiley-VCH.

3.2 Chemical reduction of graphene oxide

Chemical exfoliation of graphite is an attractive route to mass production of graphene at low cost. The presence of carboxyl-acid, phenolic-hydroxyl, and epoxide groups allows them to be stably dispersed in water and some polar organic solvents (*i.e.*, DMF, NMP, and THF).[115] On the other hand, these oxide groups disrupt the sp^2-bonding of aromatic rings, create a lot of structural defects on graphene, and result in poor electrical properties. Therefore, the post-treatment that involves the removal of these oxide groups by thermal or chemical methods to partially recover the electrical properties of graphene is of key importance. Thermal reduction of GO at high temperature (>1000 °C) can effectively decrease the oxide groups, which is performed under an Ar and H_2 atmosphere or an ultra-high vacuum, with which the oxide groups are removed in the form of CO_2, thereby leading to a nearly 80% reduced GO.[116–119] The high temperature needed for thermal reduction of GO limits the range of device substrate that can be used or requires additional transfer processes for device fabrication. Chemical reduction of GO using strong reducing agents (*i.e.*, sodium hydride, sodium borohydride, hydrazine and its derivatives) appears to be a viable method to reduce the GO resistance. During the hydrazine reduction process, hydrazine undergoes a ring-opening reaction with epoxides and forms hydrazine alcohols, which will then thermally eliminate diimide to form a double bond,[72] resulting in partial reestablishment of a conjugated graphene network, as illustrated in the following:

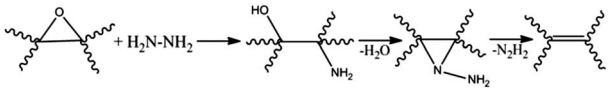

The carboxylic acid groups are unlikely to be reduced by hydrazine and thus remain intact after the hydroxyl reduction.[72,120] One of the major disadvantages is that the strong reducing-agent hydrazine is explosive and toxic.[78,121–123] New reduction methods using much less toxic reducing agents are then developed. For example, rGO reduced by *p*-toluenesulfonyl hydrazide is better suited to replace PEDOT:PSS due to its largely improved carrier transport property as well as the use of a less toxic reducing agent.[90] Either thermal reduction or chemical reduction will not heavily alter the film morphology of GO, and the overall roughness of rGO is comparable to that of as-prepared GO films.[97] As chemical reduction is less effective than thermal reduction, a combination of these two methods (*i.e.*, hydrazine reduction in conjunction with thermal reduction under Ar at 400 °C) is employed.[97,124]

3.3 Tuning the work function

In polymer BHJ solar cells, the inherent potential field induced by the work function differences between the two electrodes drives the holes and electrons towards the respective electrodes.[36] The work function of the anode electrode needs to be appropriately aligned with the HOMO level of the polymer donor (*i.e.*, ~4.8 to 5.2 eV for P3HT) to facilitate the collection of holes, while the work function of the cathode electrode should be low to match the LUMO level of the acceptor (*i.e.*, ~3.4 to 3.9 eV for PCBM) to minimize the energy barrier for electron collection.[125] As a result, the series resistance reduces, the shunt resistance increases, and in turn the device efficiency will be largely improved. The work function of GO is ~4.7 eV, which aligns well with the HOMO level of P3HT, and thus it serves as a good alternative anode buffer layer to replace PEDOT:PSS in P3HT-based solar cells. But the work function of graphene is ~4.2 to 4.5 eV and does not present a match with the HOMO level of P3HT and the LUMO level of PCBM.[51] Clearly, control over the work function of graphene is crucial in improving the performance of graphene electrodes.

The work function of graphene electrodes can be measured using Kelvin probe force microscopy (KFM) based on the difference in electrostatic force between the AFM tip and the electrode, as KFM is an effective tool to investigate the possible shift of the vacuum level at the interface or a change of work function induced by the formation of dipoles.[126] Several strategies have been proposed to adjust the work function of graphene by (a) the effect of electric field to shift the Fermi level of graphene based on the electric field-induced modulation of the carrier concentration;[127] (b) the use of metal contacts to cause the Fermi level to move away from the conical points;[128] (c) the modification of the graphene surface with an interfacial layer to form interface dipoles;[129] and (d) the chemical doping.[130] The work function of CVD-grown graphene was successfully increased to 4.7 eV after the non-covalent functionalization of graphene surface using pyrene butanoic acid succinimidyl ester (PBASE).[131] Graphene modified by PBASE exhibited improved photovoltaic characteristics in P3HT:PCBM solar cells. In comparison to the pristine graphene (PCE = 0.74%), the highest performance with V_{oc} of 0.55 V, J_{sc} of 6.05 mA cm^{-2}, FF of 51.3%, and PCE of 1.71% was achieved. The work function of graphene was also reduced by the formation of interfacial dipoles pointing away from the graphene surface. The work function of graphene was appropriately tuned from 4.5 eV to 4.2 eV by depositing different polar layers, leading to the highest PCE of 1.23% in the inverted P3HT:PCBM solar cell.[129] The doped alkali carbonates can also form interfacial dipoles on the GO surface to decrease the work function. For example, in GO/CNT nanocomposite electrodes, the work function can be tuned from 5.1 eV to 4.6 eV by doping with Li_2CO_3, 4.4 eV by doping with Na_2CO_3, 4.1 eV by doping with K_2CO_3, 3.7 eV by doping with Rb_2CO_3, and 3.4 eV by doping with Cs_2CO_3; the device incorporating the Cs_2CO_3-doped GO as the cathode yielded the highest PCE of 1.13% in inverted P3HT:PCBM solar cells (Fig. 8).[132] Very recently, an intriguing charge neutralization of the carboxylic acid groups on the GO using Cs_2CO_3 has been developed to alter the work function, making GO and Cs_2CO_3-doped GO useful as both the anode and cathode buffer layers in polymer BHJ solar cells.[133] The GO had the work function of 4.7 eV, which matched the HOMO level of P3HT for hole extraction, while the work function of Cs_2CO_3-doped GO was reduced to 4.0 eV, which matched the LUMO level of PCBM for electron extraction. The resulting P3HT:PCBM

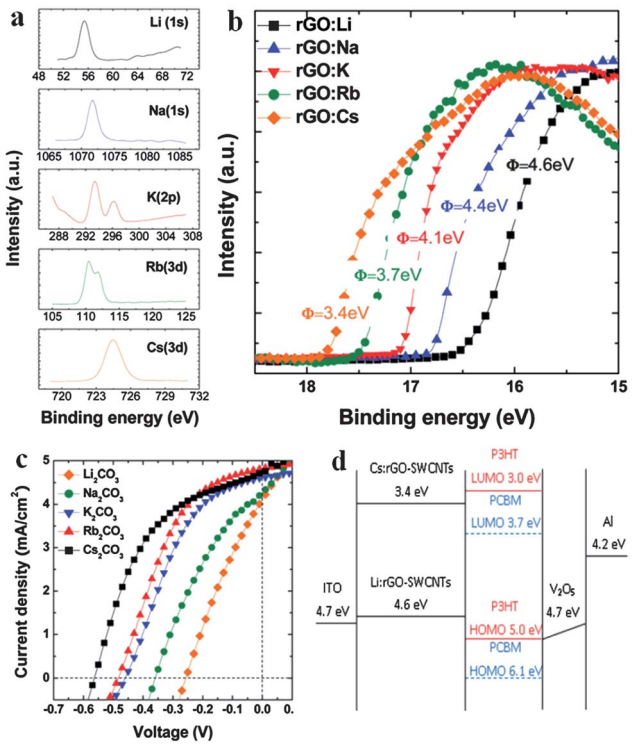

Fig. 8 Measurement of the work function of GO–SWCNT films after being doped with various alkali carbonates. (a) XPS and (b) UPS spectra of the GO doped with various alkali carbonates. (c) Current density–voltage (*J*–*V*) characteristics of the inverted P3HT/PCBM solar cells incorporating GO–SWCNT doped with various alkali carbonates as the cathode. (d) Energy level diagrams of inverted solar cells, featuring alkali carbonate-doped carbon-based cathodes. Adapted with permission from ref. 132, Copyright© 2011 American Chemical Society.

device exploiting GO as the anode buffer layer and Cs_2CO_3-doped GO as the cathode buffer layer showed a high PCE of 3.67%.[133]

4. Conclusions and outlook

The development of graphene and its derivatives as transparent flexible electrodes is of great technological importance for lightweight, flexible polymer solar cells. Graphene electrodes have partially substituted ITO in P3HT:PCBM solar cells and exhibited a high PCE of ~3% and a remarkably stable performance under bending/tensile conditions. The P3HT:PCBM solar cells capitalizing on GO as the anode/cathode buffer layer have demonstrated the performance and stability comparable to those using PEDOT:PSS as the buffer layer. Obviously, the unique properties of graphene (*i.e.*, optical transmittance, electrical conductivity, chemical stability, and flexibility) make it a promising candidate for next generation electrode materials with low cost, high performance, chemical stability, and flexibility. To better fulfill these comprehensive requirements, several strategies will most likely be employed for the future development of graphene electrodes.

4.1 Synthesis of high-quality graphene

Synthesis of high-quality graphene with minimized structural defects and organic residues needs to be further explored. The defect-free pristine graphene prepared by mechanical exfoliation using the "Scotch-tape" method shows exceptional properties, but this method is not appropriate for large-scale device fabrication. One of the critical efforts for the future research should be directed towards the synthesis of large-area, high-quality, homogenous graphene films in a well-controlled and low-cost manner. The CVD-grown graphene with a few defects satisfies several basic requirements in terms of optical transmittance, electrical conductivity, and flexibility. Future efforts to produce a large-scale graphene by CVD from various precursors and to facilitate the film-transferring process would enormously promote the applications of graphene materials. Graphene prepared by the chemical reduction of GO still suffers from poor performance due to the incorporation of oxide groups. In this context, new reducing agents are being explored to completely restore the sp^2 carbon network in rGO, yielding high-quality rGO with advanced electrical properties.

4.2 Interface engineering on graphene electrodes

The ability to tune the surface affinity, electrical conductivity, and work function of graphene electrodes offers a potentially viable route to better device performance. The interfacial layer between graphene and the photoactive layer needs to meet the requirements of close contact, energy matching, and stability in varied environments. More attention should be paid to the surface of GO electrodes, wherein the oxide-group defects, film wrinkling, and interlayer overlapping need to be well controlled. Interface engineering of graphene in terms of modifying its work function, surface free energy, and bandgap is an important aspect in the future of graphene-based electronics.

4.3 Development of hybrid electrodes

Optimization of optical and electrical properties of graphene electrodes by mixing with inorganic nanomaterials to form a hybrid electrode is also feasible in developing flexible transparent electrodes. Owing to the good solubility of GO in aqueous and polar solvents, solution blending is the best technique to prepare graphene-based nanocomposites. It has been demonstrated that the hybrid film of GO and carbon nanotubes worked well as an interconnecting layer (*i.e.*, the buffer layer) in polymer tandem solar cells.[134] Recently, the poor contact between the electrode and the photoactive layer has been resolved by directly depositing ZnO nanorods on the graphene film; the high electron affinity, carrier mobility, and favorable work function of ZnO effectively improved the charge-collecting ability of graphene electrodes.[135,136]

Acknowledgements

We gratefully acknowledge the support from Georgia Institute of Technology.

Notes and references

1 M. Law, L. E. Greene, J. C. Johnson, R. Saykally and P. D. Yang, *Nat. Mater.*, 2005, **4**, 455.
2 Y. M. Sun, G. C. Welch, W. L. Leong, C. J. Takacs, G. C. Bazan and A. J. Heeger, *Nat. Mater.*, 2012, **11**, 44.
3 T. Daeneke, T. H. Kwon, A. B. Holmes, N. W. Duffy, U. Bach and L. Spiccia, *Nat. Chem.*, 2011, **3**, 211.
4 Y. Y. Liang, Z. Xu, J. B. Xia, S. T. Tsai, Y. Wu, G. Li, C. Ray and L. P. Yu, *Adv. Mater.*, 2010, **22**, E135.
5 G. Li, V. Shrotriya, J. S. Huang, Y. Yao, T. Moriarty, K. Emery and Y. Yang, *Nat. Mater.*, 2005, **4**, 864.
6 S. Gunes, H. Neugebauer and N. S. Sariciftci, *Chem. Rev.*, 2007, **107**, 1324.
7 M. He, F. Qiu and Z. Q. Lin, *J. Mater. Chem.*, 2011, **21**, 17039.
8 F. C. Krebs, S. A. Gevorgyan and J. Alstrup, *J. Mater. Chem.*, 2009, **19**, 5442.
9 M. Singh, H. M. Haverinen, P. Dhagat and G. E. Jabbour, *Adv. Mater.*, 2010, **22**, 673.
10 G. Yu, J. Gao, J. C. Hummelen, F. Wudl and A. J. Heeger, *Science*, 1995, **270**, 1789.
11 A. C. Arango, L. R. Johnson, V. N. Bliznyuk, Z. Schlesinger, S. A. Carter and H. H. Horhold, *Adv. Mater.*, 2000, **12**, 1689.
12 P. L. T. Boudreault, A. Najari and M. Leclerc, *Chem. Mater.*, 2011, **23**, 456.
13 M. C. Scharber, D. Wuhlbacher, M. Koppe, P. Denk, C. Waldauf, A. J. Heeger and C. L. Brabec, *Adv. Mater.*, 2006, **18**, 789.
14 X. N. Yang, J. Loos, S. C. Veenstra, W. J. H. Verhees, M. M. Wienk, J. M. Kroon, M. A. J. Michels and R. A. J. Janssen, *Nano Lett.*, 2005, **5**, 579.
15 B. C. Thompson and J. M. J. Frechet, *Angew. Chem., Int. Ed.*, 2008, **47**, 58.
16 M. He, W. Han, J. Ge, Y. L. Yang, F. Qiu and Z. Q. Lin, *Energy Environ. Sci.*, 2011, **4**, 2894.
17 M. He, W. Han, J. Ge, W. J. Yu, Y. L. Yang, F. Qiu and Z. Q. Lin, *Nanoscale*, 2011, **3**, 3159.
18 M. He, L. Zhao, J. Wang, W. Han, Y. L. Yang, F. Qiu and Z. Q. Lin, *ACS Nano*, 2010, **4**, 3241.
19 C. E. Small, S. Chen, J. Subbiah, C. M. Amb, S. W. Tsang, T. H. Lai, J. R. Reynolds and F. So, *Nat. Photonics*, 2012, **6**, 115.
20 Y. Y. Liang and L. P. Yu, *Acc. Chem. Res.*, 2010, **43**, 1227.
21 Z. C. He, C. M. Zhong, X. Huang, W. Y. Wong, H. B. Wu, L. W. Chen, S. J. Su and Y. Cao, *Adv. Mater.*, 2011, **23**, 4636.
22 O. Inganas, *Nat. Photonics*, 2011, **5**, 201.
23 H. Kim, C. M. Gilmore, A. Pique, J. S. Horwitz, H. Mattoussi, H. Murata, Z. H. Kafafi and D. B. Chrisey, *J. Appl. Phys.*, 1999, **86**, 6451.

24 R. B. H. Tahar, T. Ban, Y. Ohya and Y. Takahashi, *J. Appl. Phys.*, 1998, **83**, 2631.
25 M. P. de Jong, L. J. van IJzendoorn and M. J. A. de Voigt, *Appl. Phys. Lett.*, 2000, **77**, 2255.
26 Y. Park, V. Choong, Y. Gao, B. R. Hsieh and C. W. Tang, *Appl. Phys. Lett.*, 1996, **68**, 2699.
27 X. J. Wan, G. K. Long, L. Huang and Y. S. Chen, *Adv. Mater.*, 2011, **23**, 5342.
28 J. K. Wassei and R. B. Kaner, *Mater. Today*, 2010, **13**, 52.
29 S. De, T. M. Higgins, P. E. Lyons, E. M. Doherty, P. N. Nirmalraj, W. J. Blau, J. J. Boland and J. N. Coleman, *ACS Nano*, 2009, **3**, 1767.
30 W. Gaynor, G. F. Burkhard, M. D. McGehee and P. Peumans, *Adv. Mater.*, 2011, **23**, 2905.
31 D. S. Leem, A. Edwards, M. Faist, J. Nelson, D. D. C. Bradley and J. C. de Mello, *Adv. Mater.*, 2011, **23**, 4371.
32 S. I. Na, S. S. Kim, J. Jo and D. Y. Kim, *Adv. Mater.*, 2008, **20**, 4061.
33 M. Vosgueritchian, D. J. Lipomi and Z. A. Bao, *Adv. Funct. Mater.*, 2012, **22**, 421.
34 R. A. Hatton, A. J. Miller and S. R. P. Silva, *J. Mater. Chem.*, 2008, **18**, 1183.
35 X. Wang, L. J. Zhi, N. Tsao, Z. Tomovic, J. L. Li and K. Mullen, *Angew. Chem., Int. Ed.*, 2008, **47**, 2990.
36 H. L. Yip and A. K. Y. Jen, *Energy Environ. Sci.*, 2012, **5**, 5994.
37 L. M. Chen, Z. Xu, Z. R. Hong and Y. Yang, *J. Mater. Chem.*, 2010, **20**, 10947.
38 I. Botiz and S. B. Darling, *Mater. Today*, 2010, **13**, 42.
39 A. K. Geim and K. S. Novoselov, *Nat. Mater.*, 2007, **6**, 183.
40 M. D. Stoller, S. J. Park, Y. W. Zhu, J. H. An and R. S. Ruoff, *Nano Lett.*, 2008, **8**, 3498.
41 K. I. Bolotin, K. J. Sikes, Z. Jiang, M. Klima, G. Fudenberg, J. Hone, P. Kim and H. L. Stormer, *Solid State Commun.*, 2008, **146**, 351.
42 C. Lee, X. D. Wei, J. W. Kysar and J. Hone, *Science*, 2008, **321**, 385.
43 S. Park and R. S. Ruoff, *Nat. Nanotechnol.*, 2009, **4**, 217.
44 D. H. Wang, D. W. Choi, J. Li, Z. G. Yang, Z. M. Nie, R. Kou, D. H. Hu, C. M. Wang, L. V. Saraf, J. G. Zhang, I. A. Aksay and J. Liu, *ACS Nano*, 2009, **3**, 907.
45 Y. J. Zhang, T. Mori, L. Niu and J. H. Ye, *Energy Environ. Sci.*, 2011, **4**, 4517.
46 Y. J. Zhang, K. Fugane, T. Mori, L. Niu and J. H. Ye, *J. Mater. Chem.*, 2012, **22**, 6575.
47 E. Yoo, T. Okata, T. Akita, M. Kohyama, J. Nakamura and I. Honma, *Nano Lett.*, 2009, **9**, 2255.
48 M. Jahan, Q. L. Bao, J. X. Yang and K. P. Loh, *J. Am. Chem. Soc.*, 2010, **132**, 14487.
49 S. P. Pang, Y. Hernandez, X. L. Feng and K. Mullen, *Adv. Mater.*, 2011, **23**, 2779.
50 C. Mattevi, H. Kim and M. Chhowalla, *J. Mater. Chem.*, 2011, **21**, 3324.
51 S. Bae, H. Kim, Y. Lee, X. F. Xu, J. S. Park, Y. Zheng, J. Balakrishnan, T. Lei, H. R. Kim, Y. I. Song, Y. J. Kim, K. S. Kim, B. Ozyilmaz, J. H. Ahn, B. H. Hong and S. Iijima, *Nat. Nanotechnol.*, 2010, **5**, 574.
52 P. W. Sutter, J. I. Flege and E. A. Sutter, *Nat. Mater.*, 2008, **7**, 406.
53 A. Reina, X. T. Jia, J. Ho, D. Nezich, H. B. Son, V. Bulovic, M. S. Dresselhaus and J. Kong, *Nano Lett.*, 2009, **9**, 30.
54 R. Vitchev, A. Malesevic, R. H. Petrov, R. Kemps, M. Mertens, A. Vanhulsel and C. Van Haesendonck, *Nanotechnology*, 2010, **21**, 095602.
55 S. Marchini, S. Gunther and J. Wintterlin, *Phys. Rev. B: Condens. Matter Mater. Phys.*, 2007, **76**, 075429.
56 X. S. Li, W. W. Cai, L. Colombo and R. S. Ruoff, *Nano Lett.*, 2009, **9**, 4268.
57 X. S. Li, W. W. Cai, J. H. An, S. Kim, J. Nah, D. X. Yang, R. Piner, A. Velamakanni, I. Jung, E. Tutuc, S. K. Banerjee, L. Colombo and R. S. Ruoff, *Science*, 2009, **324**, 1312.
58 H. Park, P. R. Brown, V. Buloyic and J. Kong, *Nano Lett.*, 2012, **12**, 133.
59 A. Reina, H. B. Son, L. Y. Jiao, B. Fan, M. S. Dresselhaus, Z. F. Liu and J. Kong, *J. Phys. Chem. C*, 2008, **112**, 17741.
60 M. P. Levendorf, C. S. Ruiz-Vargas, S. Garg and J. Park, *Nano Lett.*, 2009, **9**, 4479.
61 Y. Lee, S. Bae, H. Jang, S. Jang, S. E. Zhu, S. H. Sim, Y. I. Song, B. H. Hong and J. H. Ahn, *Nano Lett.*, 2010, **10**, 490.
62 K. S. Kim, Y. Zhao, H. Jang, S. Y. Lee, J. M. Kim, K. S. Kim, J. H. Ahn, P. Kim, J. Y. Choi and B. H. Hong, *Nature*, 2009, **457**, 706.
63 R. G. Gordon, *MRS Bull.*, 2000, **25**, 52.
64 S. De and J. N. Coleman, *ACS Nano*, 2010, **4**, 2713.
65 L. G. De Arco, Y. Zhang, C. W. Schlenker, K. Ryu, M. E. Thompson and C. W. Zhou, *ACS Nano*, 2010, **4**, 2865.
66 K. S. Novoselov, A. K. Geim, S. V. Morozov, D. Jiang, Y. Zhang, S. V. Dubonos, I. V. Grigorieva and A. A. Firsov, *Science*, 2004, **306**, 666.
67 Y. Y. Lee, K. H. Tu, C. C. Yu, S. S. Li, J. Y. Hwang, C. C. Lin, K. H. Chen, L. C. Chen, H. L. Chen and C. W. Chen, *ACS Nano*, 2011, **5**, 6564.
68 X. K. Lu, M. F. Yu, H. Huang and R. S. Ruoff, *Nanotechnology*, 1999, **10**, 269.
69 S. Niyogi, E. Bekyarova, M. E. Itkis, J. L. McWilliams, M. A. Hamon and R. C. Haddon, *J. Am. Chem. Soc.*, 2006, **128**, 7720.
70 S. Stankovich, R. D. Piner, X. Q. Chen, N. Q. Wu, S. T. Nguyen and R. S. Ruoff, *J. Mater. Chem.*, 2006, **16**, 155.
71 D. Li, M. B. Muller, S. Gilje, R. B. Kaner and G. G. Wallace, *Nat. Nanotechnol.*, 2008, **3**, 101.
72 S. Stankovich, D. A. Dikin, R. D. Piner, K. A. Kohlhaas, A. Kleinhammes, Y. Jia, Y. Wu, S. T. Nguyen and R. S. Ruoff, *Carbon*, 2007, **45**, 1558.
73 W. S. Hummers and R. E. Offeman, *J. Am. Chem. Soc.*, 1958, **80**, 1339.
74 N. I. Kovtyukhova, P. J. Ollivier, B. R. Martin, T. E. Mallouk, S. A. Chizhik, E. V. Buzaneva and A. D. Gorchinskiy, *Chem. Mater.*, 1999, **11**, 771.
75 I. Jung, M. Pelton, R. Piner, D. A. Dikin, S. Stankovich, S. Watcharotone, M. Hausner and R. S. Ruoff, *Nano Lett.*, 2007, **7**, 3569.
76 J. R. Lomeda, C. D. Doyle, D. V. Kosynkin, W. F. Hwang and J. M. Tour, *J. Am. Chem. Soc.*, 2008, **130**, 16201.
77 S. Stankovich, D. A. Dikin, G. H. B. Dommett, K. M. Kohlhaas, E. J. Zimney, E. A. Stach, R. D. Piner, S. T. Nguyen and R. S. Ruoff, *Nature*, 2006, **442**, 282.
78 Y. Si and E. T. Samulski, *Nano Lett.*, 2008, **8**, 1679.
79 G. X. Wang, J. Yang, J. Park, X. L. Gou, B. Wang, H. Liu and J. Yao, *J. Phys. Chem. C*, 2008, **112**, 8192.
80 X. L. Li, H. L. Wang, J. T. Robinson, H. Sanchez, G. Diankov and H. J. Dai, *J. Am. Chem. Soc.*, 2009, **131**, 15939.
81 Y. W. Zhu, M. D. Stoller, W. W. Cai, A. Velamakanni, R. D. Piner, D. Chen and R. S. Ruoff, *ACS Nano*, 2010, **4**, 1227.
82 X. F. Gao, J. Jang and S. Nagase, *J. Phys. Chem. C*, 2010, **114**, 832.
83 T. Nakajima, A. Mabuchi and R. Hagiwara, *Carbon*, 1988, **26**, 357.
84 T. Nakajima and Y. Matsuo, *Carbon*, 1994, **32**, 469.
85 D. W. Lee, T. K. Hong, D. Kang, J. Lee, M. Heo, J. Y. Kim, B. S. Kim and H. S. Shin, *J. Mater. Chem.*, 2011, **21**, 3438.
86 F. Kim, L. J. Cote and J. X. Huang, *Adv. Mater.*, 2010, **22**, 1954.
87 Z. Y. Yin, S. Y. Sun, T. Salim, S. X. Wu, X. A. Huang, Q. Y. He, Y. M. Lam and H. Zhang, *ACS Nano*, 2010, **4**, 5263.
88 D. R. Dreyer, S. Park, C. W. Bielawski and R. S. Ruoff, *Chem. Soc. Rev.*, 2010, **39**, 228.
89 S. S. Li, K. H. Tu, C. C. Lin, C. W. Chen and M. Chhowalla, *ACS Nano*, 2010, **4**, 3169.
90 J. M. Yun, J. S. Yeo, J. Kim, H. G. Jeong, D. Y. Kim, Y. J. Noh, S. S. Kim, B. C. Ku and S. I. Na, *Adv. Mater.*, 2011, **23**, 4923.
91 H. Kim, Y. Miura and C. W. Macosko, *Chem. Mater.*, 2010, **22**, 3441.
92 J. A. Zasadzinski, R. Viswanathan, L. Madsen, J. Garnaes and D. K. Schwartz, *Science*, 1994, **263**, 1726.
93 L. Zhao and Z. Q. Lin, *Soft Matter*, 2011, **7**, 10520.
94 L. Zhao, M. Byun, J. Rzayev and Z. Q. Lin, *Macromolecules*, 2009, **42**, 9027.
95 X. L. Li, G. Y. Zhang, X. D. Bai, X. M. Sun, X. R. Wang, E. Wang and H. J. Dai, *Nat. Nanotechnol.*, 2008, **3**, 538.
96 L. J. Cote, F. Kim and J. X. Huang, *J. Am. Chem. Soc.*, 2009, **131**, 1043.
97 H. A. Becerril, J. Mao, Z. Liu, R. M. Stoltenberg, Z. Bao and Y. Chen, *ACS Nano*, 2008, **2**, 463.
98 Q. B. Zheng, W. H. Ip, X. Y. Lin, N. Yousefi, K. K. Yeung, Z. G. Li and J. K. Kim, *ACS Nano*, 2011, **5**, 6039.

99 Z. Z. Zhang and K. Chang, *Phys. Rev. B: Condens. Matter Mater. Phys.*, 2008, **77**, 235411.
100 J. Wang, X. K. Xin and Z. Q. Lin, *Nanoscale*, 2011, **3**, 3040.
101 D. Y. Pan, J. C. Zhang, Z. Li and M. H. Wu, *Adv. Mater.*, 2010, **22**, 734.
102 Y. Li, Y. Hu, Y. Zhao, G. Q. Shi, L. E. Deng, Y. B. Hou and L. T. Qu, *Adv. Mater.*, 2011, **23**, 776.
103 X. Yan, X. Cui and L. S. Li, *J. Am. Chem. Soc.*, 2010, **132**, 5944.
104 X. Yan, X. Cui, B. S. Li and L. S. Li, *Nano Lett.*, 2010, **10**, 1869.
105 I. P. Hamilton, B. S. Li, X. Yan and L. S. Li, *Nano Lett.*, 2011, **11**, 1524.
106 K. S. Novoselov, A. K. Geim, S. V. Morozov, D. Jiang, M. I. Katsnelson, I. V. Grigorieva, S. V. Dubonos and A. A. Firsov, *Nature*, 2005, **438**, 197.
107 Y. B. Zhang, Y. W. Tan, H. L. Stormer and P. Kim, *Nature*, 2005, **438**, 201.
108 V. M. Apalkov and T. Chakraborty, *Phys. Rev. Lett.*, 2006, **97**, 126801.
109 A. Kasry, M. A. Kuroda, G. J. Martyna, G. S. Tulevski and A. A. Bol, *ACS Nano*, 2010, **4**, 3839.
110 X. S. Li, Y. W. Zhu, W. W. Cai, M. Borysiak, B. Y. Han, D. Chen, R. D. Piner, L. Colombo and R. S. Ruoff, *Nano Lett.*, 2009, **9**, 4359.
111 K. K. Kim, A. Reina, Y. M. Shi, H. Park, L. J. Li, Y. H. Lee and J. Kong, *Nanotechnology*, 2010, **21**, 285205.
112 H. Park, J. A. Rowehl, K. K. Kim, V. Bulovic and J. Kong, *Nanotechnology*, 2010, **21**, 505204.
113 Z. K. Liu, J. H. Li, Z. H. Sun, G. A. Tai, S. P. Lau and F. Yan, *ACS Nano*, 2012, **6**, 810.
114 Y. Wang, S. W. Tong, X. F. Xu, B. Ozyilmaz and K. P. Loh, *Adv. Mater.*, 2011, **23**, 1514.
115 C. J. Kim, W. Khan and S. Y. Park, *Chem. Phys. Lett.*, 2011, **511**, 110.
116 C. Mattevi, G. Eda, S. Agnoli, S. Miller, K. A. Mkhoyan, O. Celik, D. Mostrogiovanni, G. Granozzi, E. Garfunkel and M. Chhowalla, *Adv. Funct. Mater.*, 2009, **19**, 2577.
117 D. Yang, A. Velamakanni, G. Bozoklu, S. Park, M. Stoller, R. D. Piner, S. Stankovich, I. Jung, D. A. Field, C. A. Ventrice and R. S. Ruoff, *Carbon*, 2009, **47**, 145.
118 S. W. Lee, C. Mattevi, M. Chhowalla and R. M. Sankaran, *J. Phys. Chem. Lett.*, 2012, **3**, 772.
119 M. J. McAllister, J. L. Li, D. H. Adamson, H. C. Schniepp, A. A. Abdala, J. Liu, M. Herrera-Alonso, D. L. Milius, R. Car, R. K. Prud'homme and I. A. Aksay, *Chem. Mater.*, 2007, **19**, 4396.
120 V. Singh, D. Joung, L. Zhai, S. Das, S. I. Khondaker and S. Seal, *Prog. Mater. Sci.*, 2011, **56**, 1178.
121 N. Mohanty, A. Nagaraja, J. Armesto and V. Berry, *Small*, 2010, **6**, 226.
122 W. Gao, L. B. Alemany, L. J. Ci and P. M. Ajayan, *Nat. Chem.*, 2009, **1**, 403.
123 X. F. Zhou and Z. P. Liu, *Chem. Commun.*, 2010, **46**, 2611.
124 J. B. Wu, H. A. Becerril, Z. N. Bao, Z. F. Liu, Y. S. Chen and P. Peumans, *Appl. Phys. Lett.*, 2008, **92**, 263302.
125 H. Ma, H. L. Yip, F. Huang and A. K. Y. Jen, *Adv. Funct. Mater.*, 2010, **20**, 1371.
126 S. H. Oh, S. I. Na, J. Jo, B. Lim, D. Vak and D. Y. Kim, *Adv. Funct. Mater.*, 2010, **20**, 1977.
127 Y. J. Yu, Y. Zhao, S. Ryu, L. E. Brus, K. S. Kim and P. Kim, *Nano Lett.*, 2009, **9**, 3430.
128 G. Giovannetti, P. A. Khomyakov, G. Brocks, V. M. Karpan, J. van den Brink and P. J. Kelly, *Phys. Rev. Lett.*, 2008, **101**, 026803.
129 G. Jo, S. I. Na, S. H. Oh, S. Lee, T. S. Kim, G. Wang, M. Choe, W. Park, J. Yoon, D. Y. Kim, Y. H. Kahng and T. Lee, *Appl. Phys. Lett.*, 2010, **97**, 213301.
130 G. Jo, M. Choe, S. Lee, W. Park, Y. H. Kahng and T. Lee, *Nanotechnology*, 2012, **23**, 112001.
131 Y. Wang, X. H. Chen, Y. L. Zhong, F. R. Zhu and K. P. Loh, *Appl. Phys. Lett.*, 2009, **95**, 063302.
132 J. H. Huang, J. H. Fang, C. C. Liu and C. W. Chu, *ACS Nano*, 2011, **5**, 6262.
133 J. Liu, Y. H. Xue, Y. X. Gao, D. S. Yu, M. Durstock and L. M. Dai, *Adv. Mater.*, 2012, **24**, 2228.
134 V. C. Tung, J. Kim and J. X. Huang, *Adv. Energy Mater.*, 2012, **2**, 299.
135 Z. Y. Yin, S. X. Wu, X. Z. Zhou, X. Huang, Q. C. Zhang, F. Boey and H. Zhang, *Small*, 2010, **6**, 307.
136 Y. J. Kim, Hadiyawarman, A. Yoon, M. Kim, G. C. Yi and C. Liu, *Nanotechnology*, 2011, **22**, 245603.